Available online at www.sciencedirect.com
ScienceDirect
Polymer 48 (2007) 3790–3800
polymer
www.elsevier.com/locate/polymer

Nanoclay-tethered shape memory polyurethane nanocomposites

Feina Cao, Sadhan C. Jana*

Department of Polymer Engineering, The University of Akron, Akron, OH 44325-0301, United States

Received 8 March 2007; received in revised form 8 April 2007; accepted 12 April 2007
Available online 21 April 2007

Abstract

The study investigated shape memory properties of nanoclay-tethered polyurethane nanocomposites. Polyurethanes based on polycaprolactone (PCL) diol, methylene diisocyanate, and butane diol and their nanocomposites of reactive nanoclay were prepared by bulk polymerization in an internal mixer and the values of shape fixity and shape recovery stress were determined as function of clay content. The melting point of the crystalline soft segment was used as the transition temperature to actuate the shape memory actions. It was seen that clay particles exfoliated well in the polymer, decreased the crystallinity of the soft segment phase, and promoted phase mixing between the hard and soft segment phases. Nevertheless, the soft segment crystallinity was enough and in some cases increased due to stretching to exhibit excellent shape fixity and shape recovery ratio. A 20% increase in the magnitude of shape recovery stress was obtained with the addition of 1 wt% nanoclay. The room temperature tensile properties were seen to depend on the competing influence of reduced soft segment crystallinity and the clay content. However, the tensile modulus measured at temperatures above the melting point of the soft segment crystals showed continued increases with clay content.

Keywords: Shape memory effects; Polyurethanes; Nanocomposites

1. Introduction

An adjustable transition temperature and higher recoverable strain of the order of 100%, compared to 10% for shape memory alloys and 1% for ceramic materials make shape memory polymers very attractive as smart materials [1–3]. Of particular interests are shape memory polyurethanes (SMPU), which are gaining increasing attention from industry and academia as smart materials due to lower cost, easy processing, and light weight [4–16]. For example, polyurethane-diacrylate [5] and polyurethane-polyallyl ester polyene [6] exhibit shape memory actions in boiling water and are used as surgical implants [7]. Thermoset and thermoplastic type polyurethane shape memory polymers find applications as self-healing synthetic leather and paint [8], as transparent lens and containers [9], as heat insulator foams [10], and as ingredients of woven and non-woven fabrics [11,12]. A US patent [13] recommended diisocyanate, polyol, and chain extender molar ratio in the range of 1.1–2.0/1.0/0.10–1.0 for best performance of shape memory polyurethane foams. Hayashi et al. [14,15] invented urethane-based transparent shape memory films for packaging. These findings were later summarized in research publications by Hayashi [15] and by Hayashi et al. [16]. Kim et al. [17–19] found that high ratio of glassy to rubbery modulus, necessary for shape memory effect [15], can be easily obtained with the use of crystalline soft segments (e.g., polycaprolactone diols) [17], ionomers (e.g., dimethylpropionic acid) [18], or mesogenic moiety (e.g., hydroxy-substituted biphenyls) [19].

A typical shape memory test cycle includes the following steps: (a) deformation above transition temperature (T_{trans}) as in Fig. 1a and b, (b) fixing of deformation by rapid cooling below T_{trans} (Fig. 1c) and (c) recovery of the original shape upon heating above T_{trans} (Fig. 1d and e). The fixing of deformation or *shape fixity* and recovery of deformation as measured by *shape recovery ratio* are derived from fixed and reversible components, respectively, the hard and soft segment phases in polyurethanes. The hard segments in thermoplastic

* Corresponding author. Tel.: +1 330 972 8293; fax: +1 330 258 2339.
E-mail address: janas@uakron.edu (S.C. Jana).

0032-3861/$ - see front matter © 2007 Elsevier Ltd. All rights reserved.
doi:10.1016/j.polymer.2007.04.027

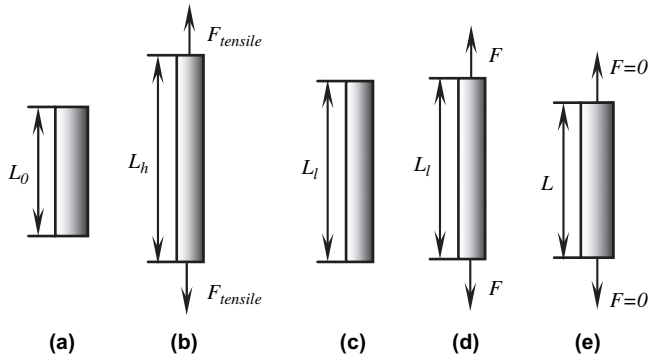

Fig. 1. Schematic showing stages in shape memory testing: (a) original state with length L_0; (b) stretched at T_{trans} to length L_h with tensile force $F_{tensile}$ and cooled to room temperature; (c) state after tensile force is released; (d) shape recovery test under constant strain; (e) unconstrained strain recovery test. Steps (d) and (e) are carried out by heating sample to T_{trans}. F is the shape recovery force.

polyurethanes contain long sequences of hydrogen bonding sites such as urethane linkages and serve as physical cross-links. These cross-link points prevent the neighboring chains from slipping past each other when subjected to deformation and consequently lead to stress buildup. On the other hand, soft segments formed by polyols undergo glass transition or melting at relatively lower temperatures. Accordingly, the soft segments can be deformed by external force at temperature, T_{trans} above the glass transition (T_g) or melting temperature (T_m), and the temporary shape can be fixed by cooling the sample below T_{trans}. Shape recovery occurs as the specimen is heated again at or above T_{trans}.

The recovery stress for shape memory polymers is usually 1–3 MPa, while that of Ti–Ni shape memory alloys is in the range 200–400 MPa [20]. Such high recovery force and almost immediate unconstrained recovery of shape memory alloys limit their usage in deployable structures due to imminent damage to auxiliary equipment. A relatively slower shape recovery of shape memory polymers provides better alternatives as materials for deployable structures, but limited recovery force is still a concern and research work on improvement of recovery force of shape memory polymers is scarce. A common approach to obtain higher recovery force is to reinforce polymers with stiffer fibers or particulate fillers with filler content often ranging between 10% and 50% by weight [21–27]. In the process, the constrained bending recovery force in SiC/epoxy shape memory composites was seen to increase by 50% with the addition of 20 wt% SiC [21]. However, it was noticed that the reinforcement itself imparted negative effects on shape recoverability, e.g., in polyurethane–carbon black system, the shape recovery ratio reduced form 98% to 65% with 30 wt% of carbon black [27]. Previous studies on thermoplastic polyurethane-exfoliated clay composites showed dramatic improvements in thermal and mechanical properties with the addition of small amounts (<10 wt%) of clay [28–33]. To the best of our knowledge, only one study reported results on shape memory polymer–clay composites in conjunction with a ternary blend of polyethylene, polyurethane, and organically modified clay [34]. It was found that the clay particles remained in intercalated state and destroyed the entanglement networks in polyurethanes. In addition, a reduction in recoverability was observed, e.g., from 78% to 57% with 5 wt% of clay. Although the tensile modulus improved in the presence of clay, the elongation at break reduced. Pattanayak and Jana [28–31] produced exfoliated clay nanocomposites of thermoplastic polyurethanes by allowing clay–polymer reactions at the time of shear mixing of reactive clay with chain-extended polymers. The same methodology was followed in this study to develop nanocomposites of shape memory polyurethanes and reactive nanoclay. A crystalline soft segment was chosen to trigger shape memory transition by the melting of the soft segment crystals. These nanocomposites offered new networks constructed by the tethered polyurethane chains onto reactive clay, which added additional constrains to chain motion on top of hydrogen bonds in the hard segment domains. The results on thermal, dynamic mechanical, and shape memory properties of these polyurethane nanocomposite materials are reported.

The current study was undertaken to answer the following questions. First, it is known that the addition of inorganic nanoscopic fillers can increase the modulus and in some cases the strength of the resultant composites. However, it is not obvious that if such increase in tensile modulus and strength automatically warrants an increase in shape recovery stress. Second, nanoparticles have been known to slow down polymer chain relaxation in nanocomposites [35]. This can be exploited to augment the shape recovery force in the resultant composites, although no previous study addressed this. Third, layered silicate clays have been known to negatively impact the extent of hard segment hydrogen bonding [28,29,36]. It becomes imperative to evaluate if this will have any impact on shape memory properties in nanoclay-filled shape memory polyurethanes.

2. Experimental

2.1. Materials

Shape memory polyurethanes were synthesized from an aromatic diisocyanate, a crystalline polyester polyol, and a short chain diol as the chain extender. Polycaprolactone diol (PCL; average molecular weight 4000 g/mol; melting temperature $T_m = 52.5\ ^\circ C$) was obtained from Solvay Chemical (Warrington, Cheshire, UK), 1,4-butane diol (BDO) was obtained from Avocado (Heysham, Lancs, UK), and 4,4′-diphenylethane diisocyanate (MDI; $T_m = 39\ ^\circ C$) was obtained from Bayer (Pittsburgh, PA). The chain extension reactions were catalyzed by dibutyltinlaureate (DABCO T120) of Air Products (Allentown, PA). Cloisite® 30B clay obtained from Southern Clay Products (Gonzales, TX) contained organic quaternary ammonium ions $N^+(CH_2CH_2OH)_2(CH_3)T$, where T represents an alkyl group with approximately 65% $C_{18}H_{37}$, 30% $C_{16}H_{33}$, and 5% $C_{14}H_{29}$. The molar ratio of isocyanate –NCO and alcoholic –OH groups was maintained at 1:1 with $-CH_2CH_2OH$ groups of the quaternary ammonium ions in Cloisite® 30B clay contributing a part of the total –OH functionality

Table 1
Molar ratio of various components of polyurethane and its nanocomposites

Material	Clay content (wt%)	Molar ratio of MDI/PCL/BDO/organic modifier[a]
PU-00	0	6/1/5.00/0
PU-01	1	6/1/4.94/0.06
PU-03	3	6/1/4.84/0.16
PU-05	5	6/1/4.72/0.28

[a] Organic modifier from Cloisite® 30B.

[25–27]. The molar ratios of various reactants in nanocomposites are listed in Table 1. The clay contents, i.e., 1 wt%, 3 wt%, 5 wt% reported in Table 1 and throughout the text represent the percentage of organic-free clay, which can be translated, respectively, to 1.3 wt%, 4.0 wt%, 6.6 wt% of Cloisite® 30B clay.

2.2. Preparation of shape memory polyurethane and its nanocomposites

The pristine polyurethane containing 33% hard segments was synthesized with a 6/1/5 molar ratio of MDI, PCL, and BDO (Table 1). The hard segment in this case was the combined weight of MDI and BDO. The prepolymer was prepared from the reaction of 6 mol MDI and 1 mol PCL (Table 1) at 80 °C for 2.5 h in a three-neck flask, equipped with nitrogen inlet and a mechanical stirrer system. The chain extension reaction between 1 mol prepolymer and 1 mol BDO was carried out in a batch mixer, Brabender Plasticorder (Model EPL 7752) at 90 °C for 25 min and was catalyzed by 2.0×10^{-7} mol/cm^3 of catalyst DABCO T120. The reaction temperature increased to 140 °C in a short time and reached a stable value at 135 °C for the rest of the reaction period. PU–clay nanocomposites were synthesized by adding desired amounts of clay to the reaction mixture after 5 min of chain extension reaction and further mixing for 20 min. This allowed reaction between –OH groups in clay with residual –NCO groups in chain-extended PU chains as was studied earlier by Pattanayak and Jana [26–29]. The temperature rose quickly to 150 °C with the addition of clay particles and then remained stable at 145 °C. The polyurethane and its nanocomposite specimens were compressed at 200–210 °C for 5 min into films with thickness of 0.4–0.5 mm, which were later used for evaluation of shape memory and mechanical properties. The molding temperatures of 200–210 °C were chosen to facilitate quick flow of the materials during compression; attempts to mold at 180 °C were unsuccessful. The compressed films were kept in vacuum oven at 40 °C for one day and then slowly cooled down to room temperature and kept for additional two days before testing.

2.3. Characterization

The thermal properties such as glass transition and melting temperatures, and heat of fusion (ΔH) of pristine polyurethane and composites were determined by differential scanning calorimetry (DSC) using TA instruments DSC (Model: DSC-29210) under nitrogen environment. The specimens were heated at a scanning rate of 10 °C/min to 250 °C and then quenched to −100 °C at an average cooling rate of 70 °C/min using liquid nitrogen. The second thermal scan was taken over a temperature range of −100–250 °C with a heating rate of 10 °C/min.

The sample specimens for Fourier transform infrared spectroscopy (FT-IR) were prepared by casting thin films on KBr discs from solutions in dimethylformamide with concentration of 10 mg/mL. These specimens were dried in vacuum oven at 80 °C for 24 h to remove the solvent. Perkin Elmer FT-IR (Model 16PC) with a resolution of 4 cm^{-1} in the range 400–4000 cm^{-1} was used to obtain FT-IR spectra of the specimens.

Dumbbell type specimens for tensile tests (ASTM D 638 type V) were prepared from compressed films using appropriate punch. Tensile tests were carried out at room temperature using an Instron universal mechanical testing machine (Model 5567) with a crosshead speed of 50 mm/min. Tensile properties were also determined at 60 °C using Instron Model 4204 tensile tester fitted with temperature controlled chamber using a crosshead speed of 20 mm/min. A minimum of five specimens were tested for each material to obtain average values and standard deviation.

Dynamic mechanical properties such as storage modulus (E') and loss modulus (E'') were determined using Perkin Elmer Instruments Pyris Diamond dynamic mechanical analyzer (DMA) in tensile mode at a frequency of 1 Hz and a heating rate of 4 °C/min from −100 °C to 100 °C. Stress relaxation experiments were also carried out in tensile mode. For this purpose, the rectangular sample was stretched at 60 °C to 100% strain at a strain rate of 20 mm/min and held at 100% strain while the stress relaxation occurred. The value of stress was monitored with time and the relaxation ratio was defined as $(\sigma_0 - \sigma_t)/\sigma_0$, with σ_0 as the initial stress and σ_t as the stress at a time t.

Wide-angle X-ray diffraction (WAXD) patterns of clay and nanocomposite specimens were generated using Rigaku X-ray diffractometer (wavelength, $\lambda = 0.154$ nm) with a tube voltage of 40 kV and tube current of 150 mA. A scanning range of $2\theta = 1.5°–10°$ was used with a scanning interval of 0.05°. Approximately 70 nm thick specimens were cut for transmission electron microscopy (TEM) using diamond knife under cryogenic condition using Reichert Ultracut S/FC S ultramicrotome (Leica). TEM images were taken using JEOL TEM device, Model: JEM-1200EXII.

Dynamic mechanical analyzer and Instron tensile testing machine (Model 4204) with temperature controlled chamber were used to determine the shape memory properties. A rectangular sample of original length L_0 (Fig. 1a) was heated to T_{trans} and elongated to a length L_h in the tensile tester with force $F_{tensile}$ at a crosshead speed of 20 mm/min (Fig. 1b). The sample with the tensile load applied on it was cooled quickly to room temperature with the aid of a fan. The temperature of the sample measured by an infrared temperature gun is shown in Fig. 2 as function of time. An instantaneous shrinkage of length from L_h to L_l occurred upon release of the load as the sample reached room temperature (Fig. 1c).

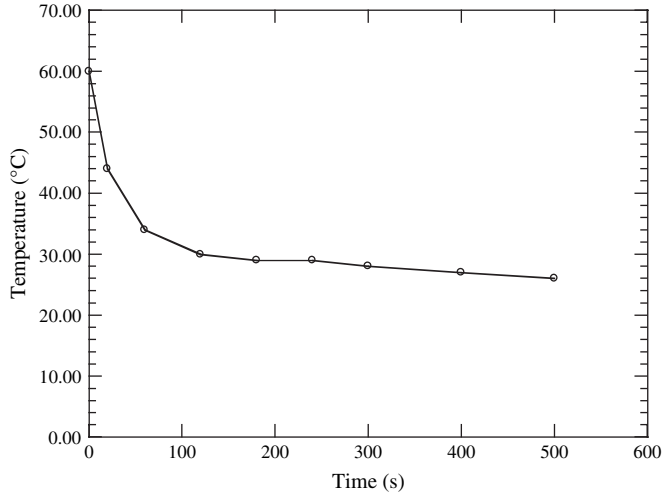

Fig. 2. Temperature vs. time during cooling process by fan. Experimental data represented by symbols are connected by straight line segments to guide the eye.

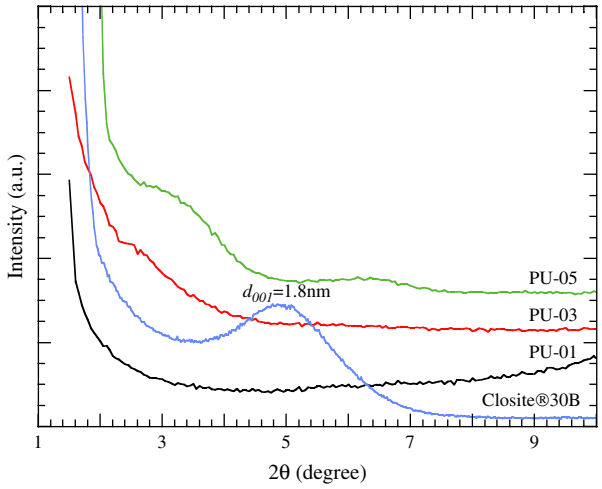

Fig. 3. WAXD patterns of Cloisite® 30B clay and polyurethane nanocomposites. Compositions are given in Table 1.

The sample lengths in different stages can be used to define *shape fixity* (f) as follows:

$$f = \frac{L_l - L_0}{L_h - L_0} \times 100\% \quad (1)$$

A value of $f = 100\%$ means no shrinkage of stretched sample upon release of tensile load. The sample of length L_l was then used in shape recovery test in DMA. In one case, the sample length was kept fixed during heating cycle and the force F required to keep the sample from shape recovery during heating at a constant rate was monitored (Fig. 1d). The value of F can be used to determine the *shape recovery stress*. Unconstrained shape recovery at constant heating rate occurred when the sample was allowed to recover to its original length against no external force, $F = 0$ (Fig. 1e). In this case, the length (L) of sample upon heating was recorded with time t and the shape recovery ratio R at time t is defined as

$$R = \frac{L - L_0}{L_l - L_0} \times 100\% \quad (2)$$

3. Results and discussion

3.1. State of clay particle dispersion

The method of nanocomposite preparation adopted in this study yielded well dispersed and well exfoliated clay structures. Fig. 3 shows WAXD patterns of Cloisite® 30B clay and PU–clay nanocomposites in the range $2\theta = 1.5°–10°$. A peak at $2\theta = 4.9°$ for curve corresponding to Cloisite® 30B clay indicates an interlayer spacing d_{001} of 1.8 nm. This peak is absent in the composite of 1 wt% clay, indicating fully exfoliated state, which is also confirmed by TEM image presented in Fig. 4a. It is seen in Fig. 4a that clay particles are dispersed to the scale of single clay layers indicated by arrows. At higher clay content, WAXD patterns of composites show small shoulders as in Fig. 3. The TEM image in Fig. 4b, corresponding to 3 wt% clay, shows both individual clay layers and sparse clay stacks, the latter with expanded d-spacing compared to $d_{001} = 1.8$ nm. The WAXD patterns for composite of 5 wt% clay (Fig. 3) show a very small peak at $2\theta = 6.5°$, and a shoulder at $2\theta = 3.4°$, which is more obvious than that with 3 wt% clay. In this case, the TEM image (Fig. 4c) reveals a combination of individual clay layers and some agglomerates of multiple clay sheets. These indicate that not all clay layers were separated from the clay tactoids, although the size of tactoids was significantly reduced, e.g., 2–3 clay sheets, compared to 200–500 clay sheets in original clay particles. Therefore, we can safely infer that clay particles in these nanocomposites were well exfoliated and well dispersed. The same observation was made in conjunction with non-shape memory polyurethane formulation [28–31]. Such excellent states of clay dispersion were anticipated to exert the following potential effects. First, it is highly likely that the clay surfaces were tethered to a large fraction of polymer chains as reported by Pattanayak and Jana [28–31]. These tethered chains may strongly interact via hydrogen bonds with $-CH_2CH_2OH$ groups in quaternary ammonium ions on clay particles. Second, the clay particles with large surface area per unit volume can potentially interact with both hard and soft segment domains and may interfere with the soft and hard segment crystallinity.

3.2. Crystallinity of soft and hard segments

As alluded to earlier, the fixed and reversible phases play key roles in determining shape memory behavior in polyurethanes. The fixed phases in this case were contributed by hydrogen bonded urethane linkages (hard segments) and possibly by the hydrogen bonded segments between the ester –CO– groups of polyol soft segments and –OH groups on quaternary ammonium ion on clay particles. On the other

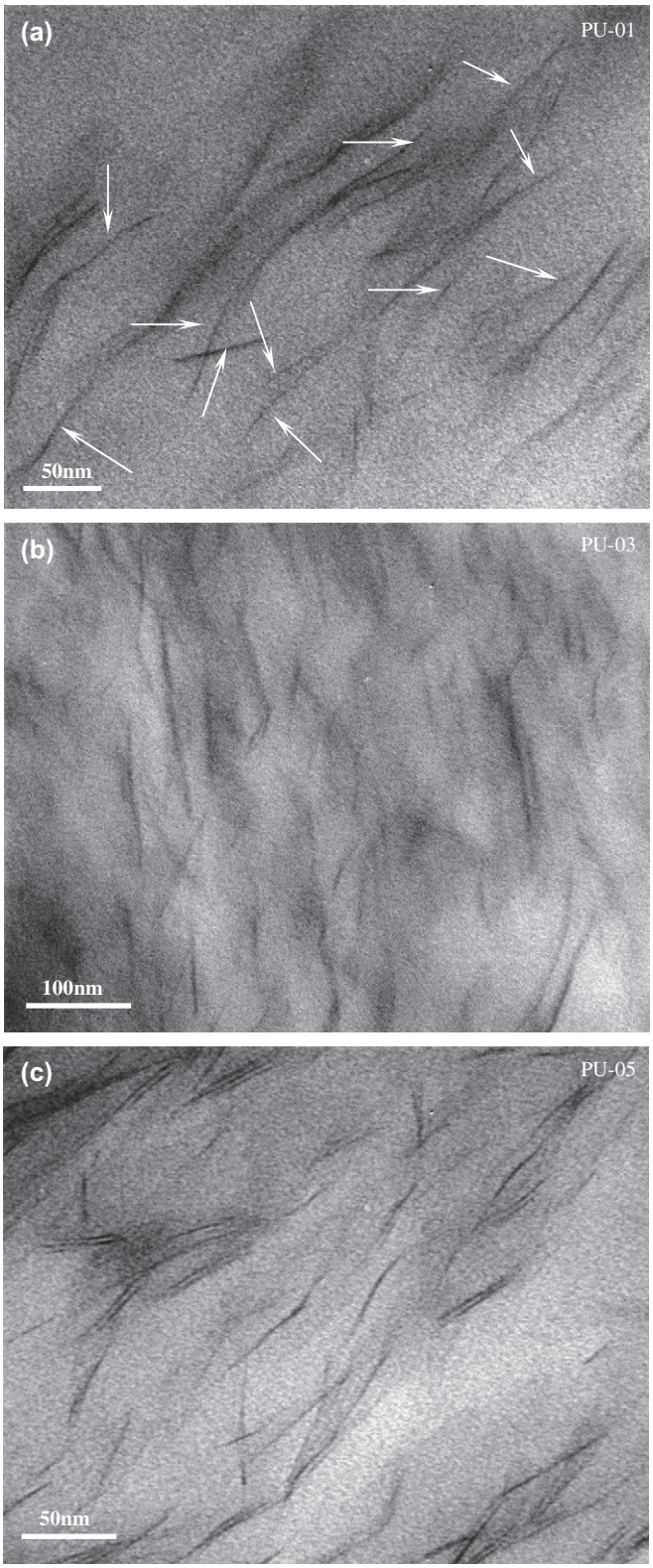

Fig. 4. TEM images of nanocomposites: (a) PU-01; (b) PU-03; (c) PU-05.

hand, the crystals of the PCL diol soft segments acted as the reversible phase. Recall that samples were deformed under tension after the crystalline reversible phase was melted at 60 °C, and the temporary shape was then frozen quickly by cooling the sample using a fan. Such cooling led to crystallization of the soft segments as the specimens were cooled below T_m. The original shape was recovered as the crystals were melted again upon heating and the soft segments went through relaxation. Thus, the crystallinity of the reversible soft segments acted as a switch for the control of the shape fixity and recoverability. It becomes imperative to study if the degree of crystallinity would be altered in the presence of nanoclay particles and exert influence on shape memory properties.

Table 2
Thermal properties of polyurethane and its nanocomposites

Material	Soft segment							Hard segment
	T_g (°C)	T_m (°C)		ΔH^a (J/g)		$\Delta H_1{}^b$ (J/g)		ΔH^c (J/g)
	2nd	1st	2nd	1st	2nd	1st	2nd	1st
PU-00	−53	45	37	19.3	16.0	28.7	23.8	9.6
PU-01	−54	43	37	16.7	15.8	25.2	23.8	5.6
PU-03	−53	42	38	15.9	14.6	24.5	22.5	6.0
PU-05	−52	41	40	12.9	11.2	20.5	17.8	4.5

1st, the first DSC scan; 2nd, the second DSC scan.
[a] Heat of fusion per gram of composite.
[b] Heat of fusion per gram PCL in composite.
[c] Heat of fusion per gram of composite.

Table 2 summarizes the values of T_g, T_m, and heat of fusion of soft segment crystals and hard segment domains of polyurethane and its clay nanocomposites from DSC traces are presented in Fig. 5. Note that the values of T_m and ΔH for soft segments were obtained from both the first and the second DSC scans, while the heat of fusion of hard segments was from the first DSC scan. The samples for first scan were subjected to the same annealing and slow cooling process, as were the samples used in the evaluation of mechanical properties and shape memory properties. In view of this, the results of the first scan were true reflection of the heat history experienced by the samples used in shape memory tests. On the other hand, the second scan was taken after quick quench. As expected, the DSC traces in Fig. 5 indicate the presence of two phases: soft segment and hard segment. The soft segment phase shows a glass transition temperature of approximately −50 °C and a melting point around 40 °C. The heat of fusion per gram of composite (ΔH) of crystalline soft segment was adjusted to heat of fusion per gram of PCL diol (ΔH_1) to obtain the origin of crystallinity from PCL diol and to compare the PCL crystallinity in various nanocomposites. The melting point and heat of fusion of pristine PCL was found to be 52 °C and 77.4 J/g, respectively. The data presented in Table 2 indicate that the crystallinity of PCL in polyurethane and its nanocomposites was much lower than that of pristine PCL. The polarized optical microscope images in Fig. 6a, show that the size of PCL crystal was up to 1 mm, while the crystal size was diminished greatly in polyurethane and its nanocomposites (Fig. 6b and c). It is also noted in Fig. 6b and c that the size of spherulites is almost independent of the presence of clay particles. As inferred from DSC data in Table 2, the crystallinity of PCL phase in nanocomposites was lower than that in pristine polyurethane. Such reduction of crystallinity of polymers in the presence of clay particles has also been

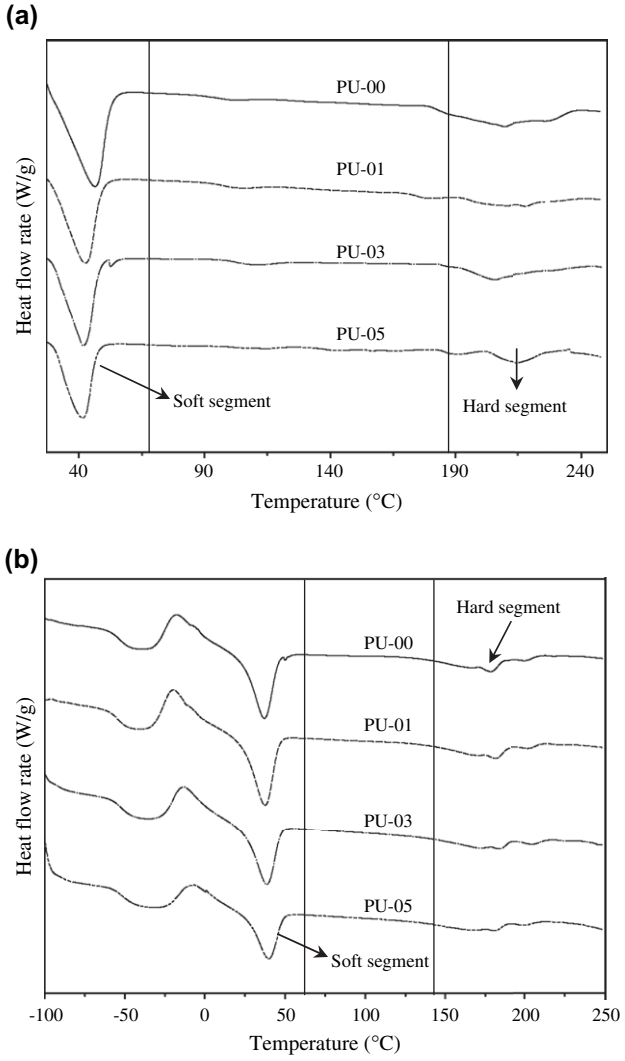

Fig. 5. DSC traces of pristine polyurethane and its nanocomposites: (a) first scan; (b) second scan.

observed by others [37–39]. One plausible argument is that PCL chains were restricted by the clay particle galleries and therefore, could not crystallize. Another argument may be higher viscosity of the clay–PCL diol mixture, which acted as a deterrent to crystallization. The same rationale can be invoked to interpret the reduction of soft segment crystallinity in nanocomposites of 1 wt% clay, although soft segment crystallinity did not reduce further when the clay content was increased to 3 wt% and 5 wt%. The hard segment crystallinity was, however, worse affected. The heat of fusion of hard segment domains decreased strongly in the presence of clay particles. This presents a possibility that the phase separation between soft and hard segments was greatly diminished in the presence of clay. Thus, a majority of the hard segments in nanocomposites remained mixed with soft segment domains, thereby resulting in a reduction of crystallinity of both PCL diol and hard segment domains. The increased phase mixing between hard and soft segment phases in the presence of nanoclay will soon become apparent from the analysis of hydrogen bonding using FT-IR.

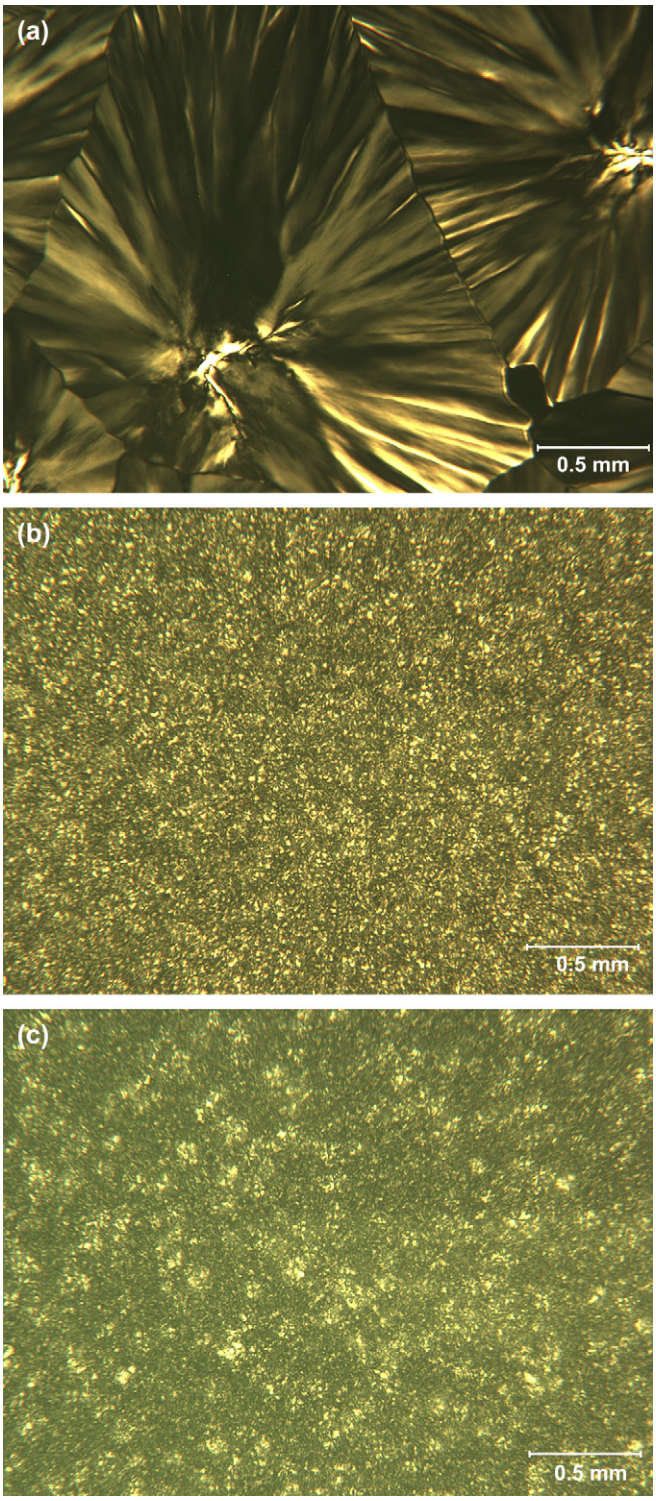

Fig. 6. Polarized optical microscope images of soft segments crystals: (a) PCL; (b) PU-00; (c) PU-01.

3.3. Analysis of hydrogen bonding

The degree of phase separation between hard and soft segment domains in polyurethanes was monitored using FT-IR spectrum. The percentage of hydrogen bonded –CO– group was used to define the degree of phase separation. In this

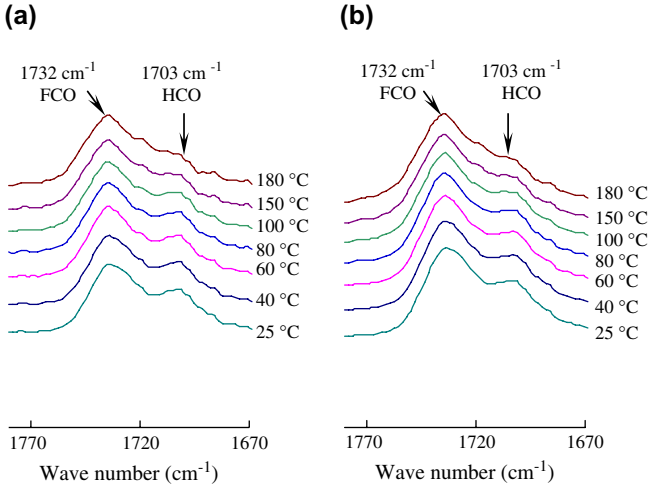

Fig. 7. FT-IR spectra of free and hydrogen bonded carbonyl peaks at different temperatures in: (a) PU-00; (b) PU-05.

case, the hydrogen bonding between −NH− and −CO− groups were followed. We focused on −CO− groups as a strong overlap of −NH− group with −OH group occurred in FT-IR spectra. In addition, its absorption coefficient is strongly frequency dependent [40]. In this work, carbonyl peak in FT-IR spectra can be attributed to both urethane linkages in hard segments and ester linkages in PCL soft segments. Thus, it was not possible to completely estimate the degree of phase separation of hard segment domains. Instead, we analyzed the effect of clay particles on hydrogen bonding as well as on thermal stability of hydrogen bonding between −CO and −NH groups to obtain information on the influence of clay particles. The peaks due to hydrogen bonded and free carbonyl groups appear at 1703 cm^{-1} and 1732 cm^{-1}, respectively [41]. As shown in Fig. 7, the FT-IR spectra of polyurethane and its nanocomposites show two peaks in the range of 1670–1800 cm^{-1}, associated with hydrogen bonded and free carbonyl groups. The ratios of areas under hydrogen bonded (A_{HCO}) and free carbonyl (A_{FCO}) groups are presented in Table 3. The value of ratio, A_{HCO}/A_{FCO}, in the nanocomposites slightly decreased compared to pristine polyurethanes. Such a decrease, although small, in the fraction of hydrogen bonded carbonyl groups can be attributed to the disturbance of phase separation of polyurethane by clay layers, which corroborates the results seen earlier in the context of crystallinity of soft and hard segment phases. The mobility of molecular chains is restricted in the presence of finely dispersed clay particles, which can lead to reduction of hard segment hydrogen bonds. As noted from DSC data, the introduction of clay particles increased phase mixing. This can be interpreted in terms of promotion of hydrogen bonding between −NH− groups in hard segment and ester −CO− groups in soft segments. Therefore, we propose the following mechanism. In the presence of clay particles, some hydrogen bonds among −NH−CO− groups in urethane linkages are disturbed. These −NH− groups instead form hydrogen bonds with −ester CO− groups from soft segments; thus, the percentage of hydrogen bonded −CO− groups remained almost the same as that of pristine polyurethanes. As a consequence, the domain size of hard segments is reduced, which results in reduced value of hard segment heat of fusion. Another possible origin of reduction of hard and soft segment domains might be, respectively, due to hydrogen bonding between urethane carbonyls or −NH− groups with unreacted $-CH_2CH_2OH$ groups on clay and between ester carbonyls with unreacted $-CH_2CH_2OH$ on clay as proposed by other investigators [28–30].

Table 3
Ratio of the areas under hydrogen bonded (A_{HCO}) and total carbonyl ($A_{FCO} + A_{HCO}$) groups

Material	PU-00	PU-01	PU-03	PU-05
$A_{HCO}/(A_{FCO}+A_{HCO})$	0.40	0.39	0.39	0.39

We also monitored hydrogen bonded carbonyls at temperatures between 25 °C and 180 °C in an effort to distinguish between various sources of hydrogen bonding. It was curious to investigate if a majority of hydrogen bonded carbonyls and hence hydrogen bonded hard segments would survive at 60 °C. Such information is essential for interpretation of both deformation (Fig. 1b) and shape recovery data obtained at 60 °C. In all cases, the intensity of free carbonyl groups increased and the intensity of hydrogen bonded carbonyl groups decreased with temperature. The ratio of areas under hydrogen bonded −CO− (A_{HCO}) and −CH stretching peak between 2700 cm^{-1} and 3100 cm^{-1} (A_{CH}) was calculated and plotted as (A_{HCO}/A_{CH}) vs. temperature (Fig. 8). It was found that A_{HCO} decreased almost linearly with temperature and that there are two different slopes, one between 25 °C and 150 °C, and the other at greater than 150 °C. Such differences in slopes may have resulted from the differences in the values of extinction coefficients as suggested by previous researchers [28,42]. The dissociation of −CO− at low temperature was mainly from the ester carbonyls while the −CO− from urethane linkages began dissociation at 150 °C. This is consistent with what was observed from DSC tests. The hard segment started to melt at temperature around 180 °C, which means the hydrogen

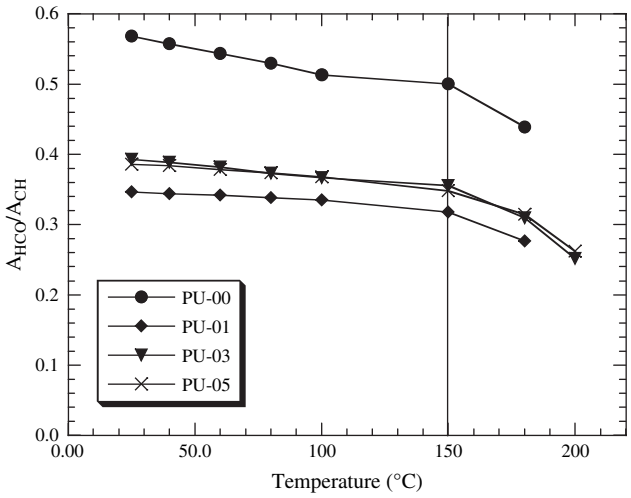

Fig. 8. Effect of temperature on hydrogen bonding.

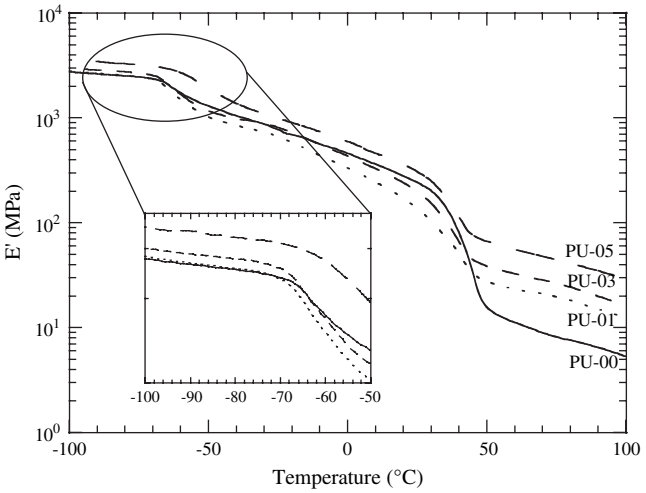

Fig. 9. Elastic modulus of polyurethane and its nanocomposites.

bonds in the large size hard segment domain remained intact below 180 °C, while in view of Fig. 8, some smaller domains started dissociation at relatively lower temperature. In view of this, it can be inferred that hard segment domains were stable at 60 °C and hence acted as the fixed phase for shape memory effects.

3.4. Mechanical properties

The elastic modulus vs. temperature data presented in Fig. 9 indicate that materials experienced glass transition and melting when the temperature was increased from −100 °C to 100 °C. Below soft segment melting temperature (~40 °C), the storage moduli of composites with 1 wt% and 3 wt% clay are lower than that for pristine PU, although it is higher in the case of 5 wt%. The moduli of nanocomposites are, however, higher than those of pristine PU above the melting temperature of soft segment, and increased with clay content. Sonnenschein et al. [43] reported that semi-crystralline soft segment in PU leads to significant modulus increase since the crystals act as reinforcements, in addition to the hard domains. In our case, the crystallinity of PCL decreased with clay content (Table 2). In view of this, the modulus at room temperature was the result of an apparent competition between decreased crystallinity in the presence of clay and reinforcement by the clay. At above 40 °C, however, the crystals of soft segments melted and the reinforcement from clay became dominant. As will be seen later, this led to an increase of modulus with clay content at temperatures greater than 60 °C.

Tensile test results at room temperature are presented in Table 5. The elastic modulus data bear the same trend as that of DMA. The tensile modulus of composite of 1 wt% clay at room temperature is lower than that of pristine PU, although an increase is observed for composite of 5 wt% clay. However, at 60 °C, the modulus increased with clay content, for example, 74%, 80% and 114% increase was observed with, respectively, 1 wt%, 3 wt% and 5 wt% clay. In addition, the nanocomposites showed an improvement in elongation at break and tensile stress – a 72% increase in ultimate stress and 35% increase in ultimate strain were observed with 1 wt% clay. Tien and Wei [33] attributed such increase to the enhancement of interfacial bonding between reactive clay and polymer chains. The mobility of molecular chains was retarded by more rigid clay particles. Additionally, the quaternary ammonium ions in clay particles potentially acted as a plasticizer, which contributes to dangling chain formation in the matrix [44]. However, with increased clay loading, i.e., 3 wt% and 5 wt%, the ultimate stress decreased. This can be attributed to better phase mixing between the soft and hard segment phases, as already discussed in conjunction with FT-IR and DSC data. This can also explain a reduction in stress at break.

3.5. Shape memory properties

The following scenarios can be anticipated to occur during preparation of sample specimens for shape memory tests. First, the chains of soft segments and the fixed hard segment phase are oriented along the direction of stretching at 60 °C. Second, the fixed hard segment phase hinders relaxation of stretched soft segment chains. Third, the soft segment upon cooling to room temperature crystallizes and provides enough restriction against relaxation of the stretched, *amorphous* soft segment (Fig. 1b). Therefore, the length of the sample was not anticipated to change much upon unloading in Fig. 1c. However, only a partial crystallization of soft segments, as revealed from the data in Table 2, could not maintain the length of the stretched sample at L_h and an immediate shrinkage of length occurred once the deformed sample was released. Moreover, the fixed phase may not have provided enough hindrance to relaxation of chains at the time of stretching. In view of this, it became imperative that the crystallinity of samples before and after stretching in Fig. 1b should be compared and used to interpret the data of shape memory tests. These data are presented in Table 4. To imitate the step in Fig. 1b, specimens were heated to 60 °C, stretched at 20 mm/min to 100% strain and then cooled down by fan to room temperature. The same cooling rate was experienced by the test specimens for shape memory tests as revealed in Fig. 2. In addition, samples were held for the same period of time at 60 °C without stretching and cooled down to room temperature, in order to have the same thermal history as the stretched samples. As noted in Fig. 2, the cooling rate was approximately 30 °C/min up to

Table 4
Comparison of heat of fusion and melting temperature of soft segment crystals of polyurethane and its nanocomposites before and after 100% elongation

Material	Heat of fusion (J/g of PCL)		Melting temperature (°C)	
	Before stretching	After stretching	Before stretching	After stretching
PU-00	34.2	45.2	45	47
PU-01	8.9	29.1	40	41
PU-03	7.4	29.6	41	43
PU-05	5.9	29.3	40	43

Table 5
Tensile properties of polyurethane and its nanocomposites

Material	At room temperature			60 °C
	Tensile modulus (MPa)	Tensile strength (MPa)	Elongation at break (%)	Tensile modulus (MPa)
PU-00	232.1 ± 11.34	24.6 ± 0.37	551.0 ± 55.88	5.7 ± 0.89
PU-01	203.0 ± 13.08	42.3 ± 0.57	742.9 ± 18.48	9.9 ± 0.24
PU-03	242.1 ± 18.90	27.2 ± 1.90	545.2 ± 17.48	10.2 ± 0.64
PU-05	302.7 ± 19.09	37.5 ± 1.44	702.8 ± 26.58	12.2 ± 0.24

a temperature of 35 °C, by which time the crystallization was nearly complete. The crystallinity of unstretched and stretched samples were determined by DSC by heating samples from room temperature to 100 °C at a scan rate of 10 °C/min, as presented in Table 4. The difference between these data and DSC data presented in Table 2 can be attributed to a much lower cooling temperature used in the latter case, −100 °C. It is noted that the heat of fusion of crystals in unstretched pristine polyurethane sample was much higher than that of nanocomposites. This is not surprising as the presence of clay in polymer matrix increased phase mixing and decreased the soft segment crystallinity as was discussed earlier. In addition, due to comparatively low crystal growth rate and short time allowed to crystallize before DSC test, the heat of fusion of unstretched nanocomposite was low. Nevertheless, the stretching process induced molecular chain alignment, which in turn facilitated additional crystallization, and thus greatly increased the heat of fusion in stretched samples. Thus, stretching-induced crystallization helped the sample fix the deformed shape, more than what was anticipated from the heat of fusion data of unstretched specimens in Table 4. The shape fixity data in Fig. 10 indicate that the addition of clay particles slightly decreased the value of shape fixity from 96% for pristine polyurethanes to 93% with 5 wt% clay. The data on crystallinity of stretched sample revealed that the heat of fusion of pristine polyurethane was higher than that of nanocomposites. Such higher crystallinity made the materials stiffer and easier to retain the stretched length once the tensile load was removed, as in Fig. 1c. This raises a question as to why pristine polyurethane samples stretched to 100% of original length shrink to 96% of its length upon removal of load. Note that the soft segments have a glass transition temperature around −50 °C, which indicates that the amorphous soft segment phase remained in rubbery state at room temperature and thus underwent immediate shrinkage after release of the tensile load, while the crystalline soft segment phase helped retain the stretched shape.

The relationship between unconstrained shape recovery ratio and temperature for polyurethane and its nanocomposites with 1 wt%, 3 wt% and 5 wt% clay is shown in Fig. 11. The melting range of soft segment crystals is also shown. It is seen that shape recovery started in all cases at 30 °C, about 10 °C below the melting temperature of the soft segments and approximately 70% deformation was recovered as the temperature reached 50 °C. Referring to DSC data in Fig. 5, this recovery range fell in the melting range of the soft segment crystals. Thus it is evident that once the crystals started melting, the amorphous chains relaxed and shape recovery began. The continued shape recovery above 50 °C came possibly from the rearrangement of amorphous molecular chains since they needed time to move from the stretched state to the original, non-deformed state. The final shape recovery ratio of pristine PU was almost 100%, and those with 1 wt% and 3 wt% clay were around 90%, for 5 wt% it was 85%. So the presence of nanoclay in PU decreased the recovery ratio as was observed for other fillers [23,26,27]. Fig. 11 also revealed that the recovery behavior of pristine PU differed significantly from that of nanocomposites in the temperature range of 40–100 °C. This difference resulted possibly from faster stress relaxation in the case of nanocomposites. This will be discussed later.

Fig. 12 shows typical recovery stress vs. temperature plot. Note that the length of the deformed sample was held constant during heating. As the soft segment crystals melted, the sample attempted to shrink and applied a compressive stress on the clamps of DMA set up. In order to keep the length constant,

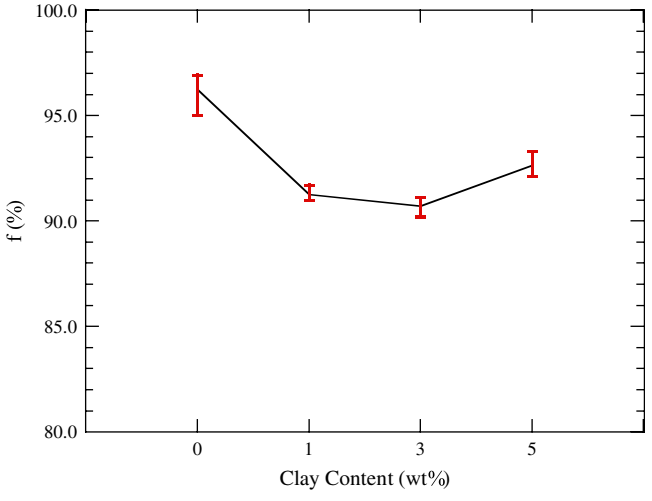

Fig. 10. Shape fixity of polyurethane and its nanocomposites. Stretching rate was 20 mm/min; stretching ratio was 2.0.

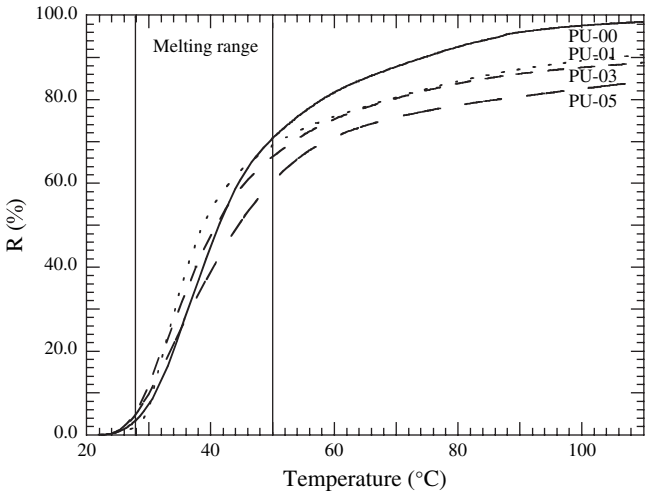

Fig. 11. Shape recovery ratio of polyurethane and its nanocomposites under unconstrained condition during heating. Heating rate was 4 °C/min.

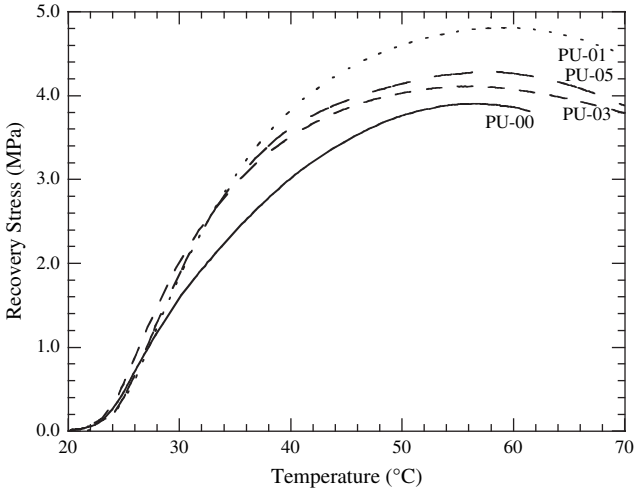

Fig. 12. Shape recovery stress of polyurethane and its nanocomposites at 100% fixed strain during heating. Heating rate was 4 °C/min.

the machine applied the same amount of stress to balance the shrinkage stress; we refer to this stress as the *recovery stress*. At the same time, the molecular chains became softer once all soft segment crystals were melted, and the material began stress relaxation. Consequently, the recovery stress declined after reaching a maximum. It is noted that the addition of clay particles improved the value of recovery stress. For example, the magnitude of recovery stress increased by 20% in the presence of 1 wt% clay. However, the peak recovery stresses of 3 wt% and 5 wt% nanocomposites are lower than those of 1 wt% case, although they are slightly larger than pristine PU. Now, two questions come to mind. Why the nanocomposites have larger recovery stress than pure polyurethane? Why the recovery stress was highest at 1 wt% loading of clay and decreased at higher clay loading? We can derive answers to these questions by reflecting on the tensile stress–strain curves obtained at 60 °C (Fig. 13). The maximum stress stored in stretched sample should correspond to the tensile stress associated with 100% strain as presented in Fig. 13. Ideally, no

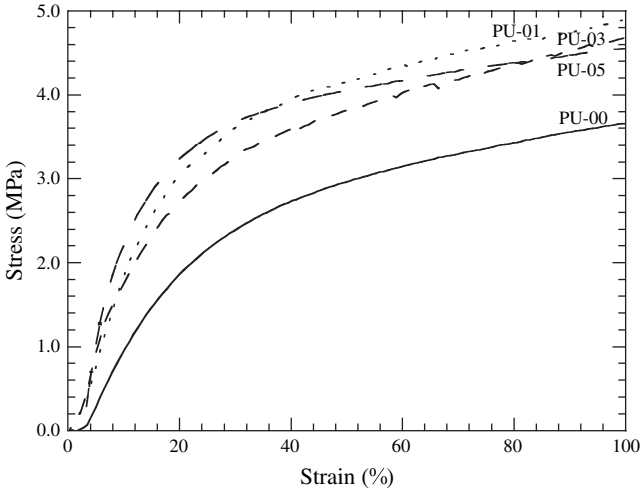

Fig. 13. Stress vs. strain during stretching at 60 °C. Stretching rate was 20 mm/min.

Table 6
Maximum stretching stress of polyurethane and its nanocomposites after 100% elongation at 60 °C

Material	PU-00	PU-01	PU-03	PU-05
Maximum stretching stress (MPa)	3.7 ± 0.15	4.9 ± 0.08	4.8 ± 0.10	4.5 ± 0.13

Stretching rate was 20 mm/min; stretching ratio was 2.0.

stress relaxation should occur during cooling of the stretched samples and the samples should not undergo shrinkage as they are released from the constraint. In view of this, the stress required to maintain constant strain should increase with temperature till a maximum stress is reached near the original tensile deformation temperature. This maximum stress should be equal to the maximum stress encountered during stretching process which in turn should present a maximum limit of the recovery stress of the sample. Table 6 presents the maximum stretching stress encountered during tensile elongation. It is seen that nanocomposites have higher values of tensile stress than pristine PU at 60 °C. Thus, the nanocomposites should also exhibit higher maximum recovery stress than pristine PU. However, it is surprising to find that the value of recovery stress for composite of 5 wt% clay is lower than those of 1 wt% and 3 wt%, although the tensile stress at 100% elongation was higher. This was probably caused by stress relaxation during the cooling step. Stress relaxation can also occur during heating at a constant strain, e.g., during shape recovery experiments. Fig. 14 shows the values of stress relaxation ratio during holding at 100% strain at 60 °C. The stress gradually decayed with hold time. This indicates that except for sample with 1 wt% clay, the nanocomposites relaxed faster than pristine PU. For example, nanocomposites of 5 wt% clay underwent 42% higher stress relaxation after 1 min than 1 wt% sample. It was earlier suggested that better exfoliation leads to lower relaxation rate and lower hysteresis loss ratio in PU–clay nanocomposites [37,45]. In our case, the best state of clay exfoliation was observed with 1 wt% clay and the relaxation rate was the lowest, resulting in the highest recovery

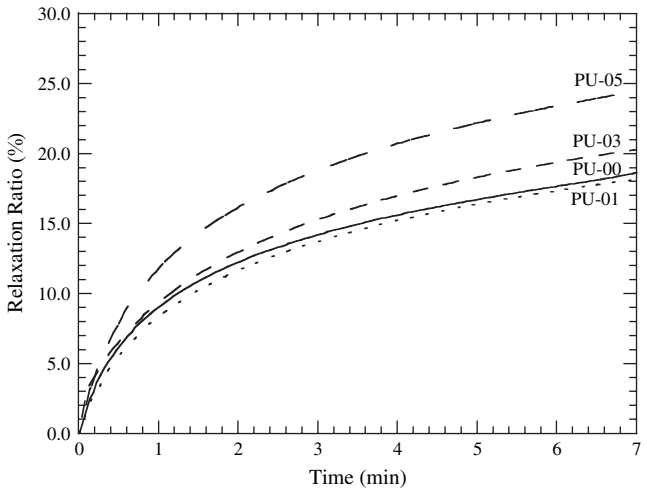

Fig. 14. Stress relaxation ratio vs. time at 60 °C.

stress. The influence of other factors, such as stretching rate, heating rate, and cooling rate also play roles in determining the maximum recovery stress. However, these were not explored in this paper.

4. Conclusions

Several conclusions can be made from this study. First, shape recovery force of shape memory polyurethanes can be increased significantly with the addition of small amounts of reactive nanoclay particles and with subsequent exfoliation. At higher clay content, more rapid relaxation of induced tensile stress limits the magnitude of maximum shape recovery force. Second, clay particles hinder soft segment crystallization and hence negatively impact the room temperature tensile properties of shape memory polyurethanes with crystalline soft segments. Third, the potential of nanoclay as reinforcing filler can be fully realized in the form of higher tensile modulus and tensile strength over pristine polyurethanes if measured at temperature above the melting point of soft segment crystals. Fourth, stretching-induced crystallization of soft segment can be exploited to obtain additional fixity of deformation in shape memory polyurethanes with crystalline soft segments.

Acknowledgment

Partial financial support for this work was provided by National Science Foundation in the form of CAREER Award (DMI-0134106) to S.C.J.

References

[1] Wei ZG, Sandstrom R. J Mater Sci 1998;33:3743.
[2] Wei ZG, Sandstrom R, Miyazaki S. J Mater Sci 1998;33:3763.
[3] Liu C, Qin H, Mather PT. J Mater Chem 2007;17:1543.
[4] Nelson GR. US Patent 3,284,275; 1966.
[5] Gould FE, Johnston CW. US Patent 4,359,558; 1982.
[6] Gould FE, Johnston CW. US Patent 4,454,309; 1984.
[7] Gould FE, Johnston CW. US Patent 4,424,305; 1984.
[8] Hourai K, Kobayashi Y, Ikegami K. US Patent 4,990,545; 1991.
[9] Hayashi S, Wakita Y. US Patent 5,135,786; 1992.
[10] Hayashi S, Ishibashi A, Ikenoue T. US Patent 5,093,384; 1992.
[11] Kobayashi K, Hayashi S. US Patent 5,098,776; 1992.
[12] Kobayashi K, Hayashi S. US Patent 5,128,197; 1992.
[13] Hayashi S, Fujimura H. US Patent 5,049,591; 1991.
[14] Hayashi S, Fujimura H, Shimizu M. US Patent 5,139,832; 1992.
[15] Hayashi S. Int Prog Urethanes 1993;6:90.
[16] Hayashi S, Kondo S, Kapadia P, Ushioda E. Plast Eng 1995;51:29.
[17] Kim BK, Lee SY, Xu M. Polymer 1996;37:5781.
[18] Kim BK, Lee SY, Lee JS, Baek SH, Choi YJ, Lee JO, et al. Polymer 1998;39:2803.
[19] Jeong HM, Lee JB, Lee SY, Kim BK. J Mater Sci 2000;35:279.
[20] Tobushi H, Hayashi S, Ikai A, Hara H. J Phys IV 1996;6:377.
[21] Gall K, Dunn ML, Liu YP, Finch D, Lake M, Munshi NA. Acta Mater 2002;50:5115.
[22] Tobushi H, Hayashi S, Hoshio K, Miwa N. Smart Mater Struct 2006;15:1033.
[23] Liang C, Rogers CA, Malafeew E. J Intell Mater Syst Struct 1997;8:380.
[24] Gall K, Mikulas M, Munshi NA, Beavers F, Tupper M. J Intell Mater Syst Struct 2000;11:877.
[25] Liu YP, Gall K, Dunn ML, McCluskey P. Mech Mater 2004;36:929.
[26] Cho JW, Lee SH. Eur Polym J 2004;40:1343.
[27] Li FK, Qi LY, Yang JP, Xu M, Luo XL, Ma DZ. J Appl Polym Sci 2000;75:68.
[28] Pattanayak A, Jana SC. Polymer 2005;46:3275.
[29] Pattanayak A, Jana SC. Polymer 2005;46:3394.
[30] Pattanayak A, Jana SC. Polymer 2005;46:5183.
[31] Pattanayak A, Jana SC. Polym Eng Sci 2005;45:1532.
[32] Chen TK, Tien YI, Wei KH. Polymer 2000;41:1345.
[33] Tien YI, Wei KH. Macromolecules 2001;34:9045.
[34] Mishra JK, Kim I, Ha CS. Macromol Rapid Commun 2004;25:1851.
[35] Wang K, Liang S, Deng J, Yang H, Zhang Q, Fu Q, et al. Polymer 2006;47:7131.
[36] Tien YI, Wei KH. Polymer 2001;42:3213.
[37] Dai XH, Xu J, Guo XL, Lu YL, Shen DY, Zhao N, et al. Macromolecules 2004;37:5615.
[38] Shen ZQ, Simon GP, Cheng YB. Polym Eng Sci 2002;42:2369.
[39] Vaia RA, Vasudevan S, Krawiec W, Scanlon LG, Giannelis EP. Adv Mater 1995;7:154.
[40] Coleman MM, Lee KH, Skrovanek DJ, Painter PC. Macromolecules 1986;19:2149.
[41] Lee HS, Wang YK, Macknight WJ, Hsu SL. Macromolecules 1988;21:270.
[42] Srichatrapimuk VW, Cooper SL. J Macromol Sci Phys 1978;B15:267.
[43] Sonnenschein MF, Lysenko Z, Brune DA, Wendt BL, Schrock AK. Polymer 2005;46:10158.
[44] Wang Z, Pinnavaia TJ. Chem Mater 1998;10:3769.
[45] Xia HS, Shaw SJ, Song M. Polym Int 2005;54:1392.